Journal of Biomedical Optics

BiomedicalOptics.SPIEDigitalLibrary.org

Development of photostabilized asymmetrical cyanine dyes for *in vivo* photoacoustic imaging of tumors

Satoru Onoe
Takashi Temma
Kengo Kanazaki
Masahiro Ono
Hideo Saji

SPIE.

Development of photostabilized asymmetrical cyanine dyes for *in vivo* photoacoustic imaging of tumors

Satoru Onoe,[a] Takashi Temma,[a,b] Kengo Kanazaki,[a,c] Masahiro Ono,[a] and Hideo Saji[a,*]
[a]Kyoto University, Graduate School of Pharmaceutical Sciences, Department of Patho-Functional Bioanalysis, 46-29 Yoshida Shimoadachi-cho, Sakyo-ku, Kyoto 606-8501, Japan
[b]National Cerebral and Cardiovascular Center Research Institute, Department of Investigative Radiology, 5-7-1 Fujishiro-dai, Suita, Osaka 565-8565, Japan
[c]Canon Inc., Corporate R&D Headquarters, Medical Imaging Project, 3-30-2 Shimomaruko, Ohta-ku, Tokyo 146-8501, Japan

Abstract. Photoacoustic imaging (PAI) contributes to tumor diagnosis through the use of PAI probes that effectively accumulate in tumors. Previously, we developed a symmetrical cyanine dye, IC7-1-Bu, which showed high potential as a PAI probe because of its high tumor targeting ability and sufficient *in vivo* PA signal. However, IC7-1-Bu lacks photostability for multiple laser irradiations, so we developed stabilized PAI probes using IC7-1-Bu as a lead compound. We focused on the effect of singlet oxygen ($^1O_2$) generated by excited PAI probes on probe degeneration. We introduced a triplet-state quencher (TSQ) moiety into IC7-1-Bu to quench $^1O_2$ generation and designed three IC-*n*-T derivatives with different linker lengths (*n* indicates linker length). The IC-*n*-T derivatives emitted *in vitro* PA signals that were comparable to IC7-1-Bu and significantly reduced $^1O_2$ generation while showing improved photostability against multiple irradiations. Of the three derivatives evaluated, IC-5-T accumulated in tumors effectively to allow clear PAI of tumors *in vivo*. Furthermore, the photostability of IC-5-T was 1.5-fold higher than that of IC7-1-Bu in *in vivo* sequential PAI. These results suggest that IC-5-T is a potential PAI probe for *in vivo* sequential tumor imaging. [DOI: 10.1117/1.JBO.20.9.096006]

Keywords: triplet-state quencher; near-infrared; photoacoustic imaging; optical imaging; albumin binding; cancer diagnosis.
Paper 150248R received Apr. 11, 2015; accepted for publication Jul. 15, 2015; published online Sep. 10, 2015.

1 Introduction

Since the number of cancer cases continues to increase,[1] the development of noninvasive imaging methods to detect cancer is very important for early diagnosis.[2] Photoacoustic imaging (PAI) using the PA effect of endogenous biomolecules or exogenous contrast agents has emerged as a new imaging technique that has developed rapidly over recent years because PAI can detect PA signals from depths of up to 5 cm with high contrast and spatial resolution.[3,4] Thus, the development of effective PA contrast agents is urgently needed for noninvasive cancer imaging.

Low molecular weight dyes with a maximum absorption wavelength in the near-infrared (NIR) region used as PAI probes would have a clear advantage over nanotechnology-based contrast agents in terms of having simple preparation, cost-effectiveness, and potentially low toxicity. Such dyes would thus have various applications in clinical settings. In our previous report, we developed a symmetrical NIR cyanine dye for use as a probe in fluorescence imaging of tumors[5] and preclinically evaluated its usefulness for cancer imaging with PAI.[6] This dye, IC7-1-Bu (2-(2-(3-(2-(3-butyl-1,1-dimethyl-1,3-dihydro-2H-benz[*e*]indol-2-ylidene)ethylidene)-2-chlorocyclohex-1-en-1-yl)vinyl)-3-butyl-1,1-dimethyl-1H-benz[*e*]indol-3-ium), accumulated to high levels in mouse tumors after intravenous injection using serum albumin as a drug carrier for tumor targeting and enabled clear tumor imaging with PAI. However, a second laser irradiation for serial observation of dye biodistribution greatly diminished the PA signals detected in tumors. This finding differed from results for another fluorescence imaging experiment using the same dye, likely because of the high-energy laser pulses needed for PAI[4] that could degrade PAI probes. These results indicated that a high photostability of PAI probes is needed for effective applications and that the photostability of IC7-1-Bu should be improved.

A PAI probe excited with a NIR pulse laser generates singlet oxygen ($^1O_2$) from triplet oxygen ($^3O_2$) in a given region, which could lead to PAI probe degeneration.[7] Therefore, to improve its photostability for serial tumor imaging studies, IC7-1-Bu could be modified by introducing a chemical moiety that can function as a triplet-state quencher (TSQ) that may reduce $^1O_2$ generation and improve dye photostability. In this study, we focused on a 4-nitrobenzyl alcohol derivative as a usable TSQ moiety[8] and synthesized a series of IC7-1-Bu derivatives conjugated with a 4-nitrobenzyl alcohol derivative (named IC-*n*-T derivatives, where *n* represents the alkyl chain length, as shown in Fig. 1). We evaluated the PA properties of these probes and their photostability in *in vitro* experiments. We next investigated their usefulness as tumor imaging agents using tumor-bearing mice and an *in vivo* PAI modality.

*Address all correspondence to: Hideo Saji, E-mail: hsaji@pharm.kyoto-u.ac.jp

1083-3668/2015/$25.00 © 2015 SPIE

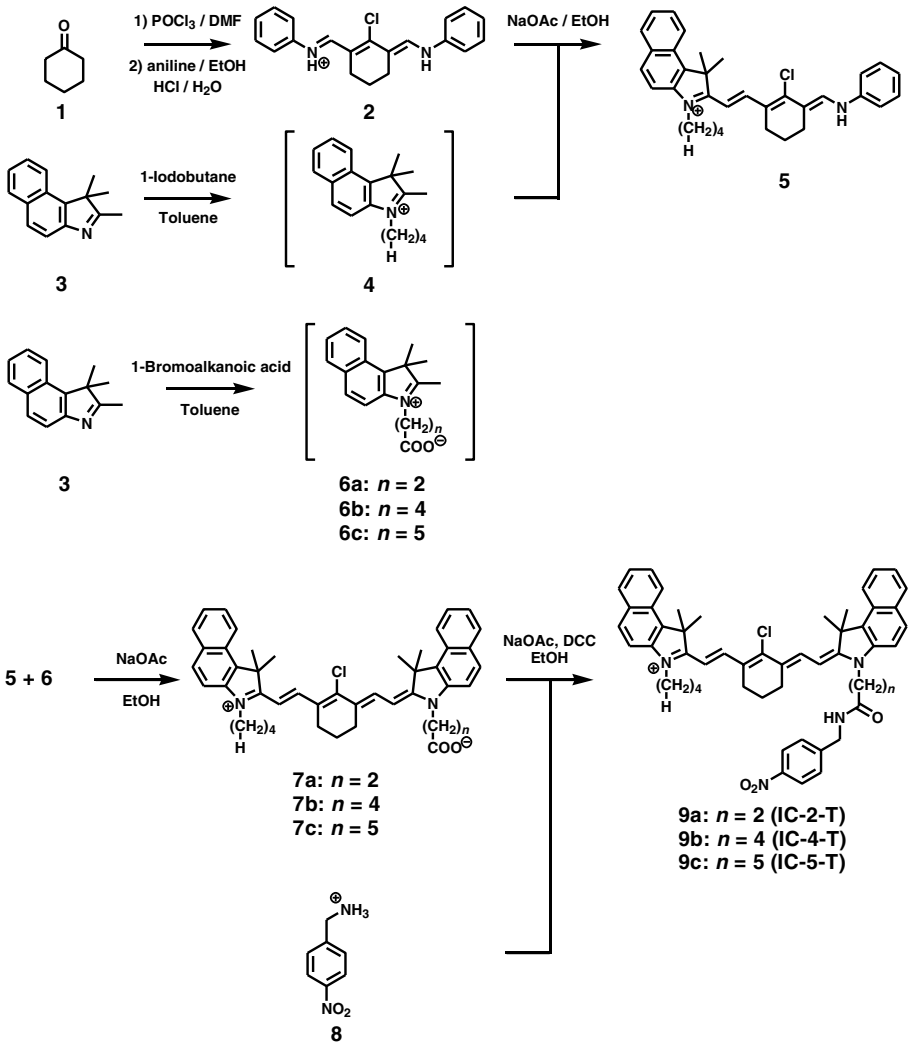

Fig. 1 Synthesis of IC-*n*-T derivatives.

2 Materials and Methods

2.1 *Materials*

All reagents were purchased from Wako Pure Chemical Industries, Ltd. (Osaka, Japan), Tokyo Chemical Industry Co., Ltd. (Tokyo, Japan), or Nacalai Tesque Inc. (Kyoto, Japan) and were used without further purification. For cell experiments, Dulbecco's modified Eagle's medium (DMEM) and fetal bovine serum (FBS) were purchased from Nissui Pharmaceutical Co., Ltd. (Tokyo, Japan) and Nichirei Co. (Tokyo, Japan), respectively. D10001 was purchased from Research Diets, Inc. (New Brunswick, New Jersey).

2.2 *Instruments*

^{1}H-nuclear magnetic resonance (NMR) spectra were recorded on a JEOL ECP-400 apparatus (JEOL Ltd., Tokyo, Japan). Mass spectra and high-resolution mass spectra (HRMS) were acquired on a Shimadzu LC-MS2010 EV spectrometer (Shimadzu Co., Kyoto, Japan) and JEOL JMS-SX 102A QQ spectrometer (JEOL Ltd.), respectively. UV-vis spectra were measured using a UV-1800 spectrometer (Shimadzu Co.). Fluorescence spectroscopy was performed with a Fluorolog-3 device equipped with a NIR sensitive photomultiplier detection system (~1200 nm) (HORIBA Jobin Yvon Inc., Kyoto, Japan) and a slit width of 5 nm for excitation and emission measurements.

2.3 *Synthesis*

N-[5-anilino-3-chloro-2,4-(propane-1,3-diyl)-2,4-pentadiene-1-ylidene]anilinium chloride (**2**) and 3-butyl-1,1,2-trimethyl-1H-benz[*e*]indol-3-ium (**4**) was prepared as reported previously (Fig. 1).[5]

2.3.1 *N-((3-(2-(3-butyl-1,1-dimethyl-1,3-dihydro-2H-benz[e] indol-2-ylidene)ethylidene)-2-chlorocyclohex-1-en-1-yl) methylene)benzenaminium (5)*

Compound **4** (500 mg, 1.3 mmol) and anhydrous sodium acetate (NaOAc, 125 mg, 1.5 mmol) were added to compound **2** (456 mg, 1.3 mmol), dissolved in ethanol (EtOH, 12 mL), and the mixture was refluxed for 3 h. After completion of the reaction, the mixture was cooled to room temperature and the solvent was evaporated. The reaction mixture was partitioned between chloroform ($CHCl_3$) and water (H_2O), and the organic layer was separated, washed with brine, dried over anhydrous sodium sulfate

(Na_2SO_4), and concentrated under vacuum. The residue was purified by column chromatography to obtain compound **5**, which was a dark-red solid (76 mg, 12%). ^{1}H NMR ($CDCl_3$) δ 8.74 (s, 1H), 8.08 to 7.83 (m, 4H), 7.55 to 7.37 (m, 6H), 7.23 to 7.20 (m, 2H), 3.01 (s, 1H), 2.63 (t, $J = 5.9$, 2H), 1.99 to 1.42 (m, 18H), 1.03 (t, $J = 7.3$, 3H): MS (ESI, pos) m/z calcd. for $C_{33}H_{36}ClN_2$ (M+): 495, detected: 495.

2.3.2 *General procedure for the synthesis of 2-(2-(3-(2-(3-butyl-1,1-dimethyl-1,3-dihydro-2H-benz[e]indol-2-ylidene)ethylidene)-2-chlorocyclohex-1-en-1-yl)vinyl)-3-carboxyalkyl-1,1-dimethyl-1H-benz[e]indol-3-ium 7a to 7c*

1,1,2-Trimethyl-1H-benz[*e*]indole (1.1 g, 5.2 mmol) was added to bromoalkanoic acid (15.5 mmol) dissolved in toluene (1.5 mL), and the mixture was refluxed for 12 h. The resulting precipitate was washed with tetrahydrofuran, ether, and $CHCl_3$ and then dried under vacuum. The product (compound **7**) was used for the next reaction without further purification. Compound **6** (0.061 mmol) was mixed with compound **5** (30 mg, 0.061 mmol) and NaOAc (6 mg, 0.072 mmol) in EtOH (600 μL), and the mixture was refluxed for 3 h. After completion of the reaction, the mixture was cooled to room temperature and the solvent was evaporated. The reaction mixture was partitioned between $CHCl_3$ and H_2O, and the organic layer was separated, washed with brine, dried over anhydrous Na_2SO_4, and concentrated under vacuum. The residue was purified by column chromatography to obtain compounds **7a** to **7c**.

2-(2-(3-(2-(3-butyl-1,1-dimethyl-1,3-dihydro-2H-benz[e]indol-2-ylidene)ethylidene)-2-chlorocyclohex-1-en-1-yl)vinyl)-3-(2-carboxyethyl)-1,1-dimethyl-1H-benz[e]indol-3-ium (7a). **7a** was obtained from 3-bromopropionic acid as a dark-green solid (21 mg, 43%). ^{1}H NMR ($CDCl_3$) δ 8.52 (d, $J = 14$ Hz, 1H), 8.42 (d, $J = 14$ Hz, 1H), 8.13 (d, $J = 8.5$ Hz, 2H), 7.98 to 7.92 (m, 4H), 7.63 to 7.60 (m, 2H), 7.54 to 7.32 (m, 4H), 6.51 (d, $J = 14$ Hz, 1H), 6.05 (d, $J = 14$ Hz, 1H), 4.61 (t, $J = 6.6$ Hz, 2H), 4.10 (t, $J = 7.4$ Hz, 2H), 3.05 (t, $J = 6.6$ Hz, 2H), 2.77 (t, $J = 5.3$ Hz, 2H), 2.66 (t, $J = 5.3$ Hz, 2H), 2.03 to 1.99 (m, 14H), 1.91 to 1.83 (m, 2H), 1.56-1.47 (m, 2H), 1.05 (t, $J = 7.3$, 3H): MS (ESI, pos) m/z calcd. for $C_{45}H_{47}ClN_2O_2$ (M+): 683, detected: 683.

2-(2-(3-(2-(3-butyl-1,1-dimethyl-1,3-dihydro-2H-benz[e]indol-2-ylidene)ethylidene)-2-chlorocyclohex-1-en-1-yl)vinyl)-3-(2-carboxybutyl)-1,1-dimethyl-1H-benz[e]indol-3-ium (7b). **7b** was obtained from 5-bromovaleric acid as a dark-green solid (15 mg, 30%). ^{1}H NMR ($CDCl_3$) δ 8.53 (d, $J = 14$ Hz, 1H), 8.38 (d, $J = 14$ Hz, 1H), 8.14 to 8.11 (m, 2H), 7.99 to 7.91 (m, 4H), 7.65 to 7.59 (m, 2H), 7.53 to 7.31 (m, 4H), 6.46 (d, $J = 14$ Hz, 1H), 6.02 (d, $J = 14$ Hz, 1H), 4.36 (t, $J = 7.5$ Hz, 2H), 4.08 (t, $J = 7.4$ Hz, 2H), 2.83 to 2.80 (m, 4H), 2.67 (t, $J = 5.9$ Hz, 2H), 2.02 to 1.83 (m, 20H), 1.57 to 1.48 (m, 2H), 1.05 (t, $J = 7.3$, 3H): MS (ESI, pos) m/z calcd. for $C_{47}H_{51}ClN_2O_2$ (M+): 711, detected: 711.

2-(2-(3-(2-(3-butyl-1,1-dimethyl-1,3-dihydro-2H-benz[e]indol-2-ylidene)ethylidene)-2-chlorocyclohex-1-en-1-yl)vinyl)-3-(2-carboxypentyl)-1,1-dimethyl-1H-benz[e]indol-3-ium (7c). **7c** was obtained from 6-bromohexanoic acid as a dark-green solid (17 mg, 33%). ^{1}H NMR ($CDCl_3$) δ 8.52 (d, $J = 14$ Hz, 1H), 8.41 (d, $J = 14$ Hz, 1H), 8.13 (d, $J = 8.5$ Hz, 2H), 7.99 to 7.92 (m, 4H), 7.65 to 7.59 (m, 2H), 7.53 to 7.32 (m, 4H), 6.35 (d, $J = 14$ Hz, 1H), 6.06 (d, $J = 14$ Hz, 1H), 4.25 (t, $J = 7.4$ Hz, 2H), 4.10 (t, $J = 7.4$ Hz, 2H), 2.76 (t, $J = 5.3$ Hz, 2H), 2.68 (t, $J = 5.3$ Hz, 2H), 2.57 (t, $J = 6.7$, 2H), 2.07-1.92 (m, 20H), 1.89 to 1.81 (m, 4H), 1.61 (t, $J = 6.7$, 3H): MS (ESI, pos) m/z calcd. for $C_{48}H_{53}ClN_2O_2$ (M+): 725, detected: 725.

2.3.3 *General procedure for the synthesis of 2-(2-(3-(2-(3-butyl-1,1-dimethyl-1,3-dihydro-2H-benz[e]indol-2-ylidene)ethylidene)-2-chlorocyclohex-1-en-1-yl)vinyl)-1,1-dimethyl-3-(((4-nitrobenzyl)amino)-substituted)-1H-benz[e]indol-3-ium 9a to 9c*

Compound **8** (1 equiv) was mixed with 4-nitrobenzylamine hydrochloride (1 equiv) and N,N'-dicyclohexylcarbodiimide (DCC, 1.2 equiv) in N,N-dimethylformamide (130 to 260 μL), and the mixture was stirred at room temperature for 1 day. After completion of the reaction, the reaction mixture was partitioned between $CHCl_3$ and H_2O and the organic layer was separated, washed with brine, dried over anhydrous Na_2SO_4, and concentrated under vacuum. The residue was purified by column chromatography and reverse phase-high performance liquid chromatography (RP-HPLC) on a Cosmosil 5C_{18} column to obtain compounds **9a** to **9c**. The mobile phase of RP-HPLC was isocratic with 30% H_2O [0.1% trifluoroacetic acid (TFA)] and 70% methanol (MeOH, 0.1% TFA) at 0 to 5 min, followed by a gradient mobile phase going from 30% H_2O (0.1% TFA) and 70% MeOH (0.1% TFA) at 5 min to 0% H_2O (0.1% TFA), and 100% MeOH (0.1% TFA) at 35 min.

2-(2-(3-(2-(3-butyl-1,1-dimethyl-1,3-dihydro-2H-benz[e]indol-2-ylidene)ethylidene)-2-chlorocyclohex-1-en-1-yl)vinyl)-1,1-dimethyl-3-(3-((4-nitrobenzyl)amino)-3-oxopropyl)-1H-benz[e]indol-3-ium (9a: IC-2-T). **9a** was obtained from compound **7a** as a dark-green solid (1.2 mg, 8%). ^{1}H NMR ($CDCl_3$) δ 10.31 (bs, 1H), 8.52 (d, $J = 14$ Hz, 1H), 8.35 (d, $J = 14$ Hz, 1H), 8.12 (d, $J = 7.9$ Hz, 2H), 7.96 to 7.90 (m, 6H), 7.70 to 7.28 (m, 8H), 6.55 (d, $J = 14$ Hz, 1H), 5.96 (d, $J = 14$ Hz, 1H), 4.67 (t, $J = 6.8$ Hz, 2H), 4.44 (d, $J = 5.8$ Hz, 2H), 4.05 (t, $J = 7.5$, 2H), 3.11 (t, $J = 6.8$ Hz, 2H), 2.71 (t, $J = 5.9$ Hz, 2H), 2.63 (t, $J = 5.9$ Hz, 2H), 2.03-1.84 (m, 16H), 1.56-1.48 (m, 2H), 1.06 (t, $J = 7.3$, 3H); MS (ESI, pos) m/z calcd. for $C_{52}H_{54}ClN_4O_3$ (M+): 817, detected: 817; HRMS (FAB) m/z calcd. for $C_{54}H_{58}ClN_4O_3$ (M+): 817.39, detected: 817.3884.

2-(2-(3-(2-(3-butyl-1,1-dimethyl-1,3-dihydro-2H-benz[e]indol-2-ylidene)ethylidene)-2-chlorocyclohex-1-en-1-yl)vinyl)-1,1-dimethyl-3-(5-((4-nitrobenzyl)amino)-5-oxopentyl)-1H-benz[e]indol-3-ium (9b: IC-4-T). **9b** was obtained from compound **7b** as a dark-green solid (1.2 mg, 7.4%). ^{1}H NMR ($CDCl_3$) δ 9.45 (bs, 1H), 8.55 (d, $J = 14$ Hz, 1H), 8.37 (d, $J = 14$ Hz, 1H), 8.14 to 8.06 (m, 4H), 8.01 to 7.91 (m, 4H), 7.66 to 7.44 (m, 8H), 6.48 (d, $J = 14$ Hz, 1H), 5.97 (d, $J = 14$ Hz, 1H), 4.55 (t, $J = 6.2$ Hz, 2H), 4.44 (t, $J = 7.0$ Hz, 2H), 4.06 (t, $J = 7.4$, 2H), 2.81 (t, $J = 5.9$ Hz, 2H), 2.72 (t, $J = 6.5$ Hz, 2H), 2.64 (t, $J = 5.9$ Hz, 2H), 2.03-1.84 (m, 20H), 1.61-1.48 (m, 2H), 1.06 (t, $J = 7.3$, 3H); MS (ESI, pos) m/z calcd. for $C_{54}H_{58}ClN_4O_3$ (M+): 845, detected: 845; HRMS

(FAB) m/z calcd. for $C_{54}H_{58}ClN_4O_3$ (M+): 845.42, detected: 845.4197.

2-(2-(3-(2-(3-butyl-1,1-dimethyl-1,3-dihydro-2H-benz[e]indol-2-ylidene)ethylidene)-2-chlorocyclohex-1-en-1-yl)vinyl)-1,1-dimethyl-3-(6-((4-nitrobenzyl)amino)-6-oxohexyl)-1H-benz[e]indol-3-ium (9c: IC-5-T).. **9c** was obtained from compound **7c** as a dark-green solid (1.0 mg, 13%). ^{1}H NMR ($CDCl_3$) δ 9.39 (bs, 1H), 8.53 (d, $J = 14$ Hz, 1H), 8.39 (d, $J = 14$ Hz, 1H), 8.14 to 8.08 (m, 4H), 7.99 to 7.92 (m, 4H), 7.65 to 7.30 (m, 8H), 6.33 (d, $J = 14$ Hz, 1H), 6.01 (d, $J = 14$ Hz, 1H), 4.52 (t, $J = 6.0$ Hz, 2H), 4.26 (t, $J = 7.3$ Hz, 2H), 4.09 (t, $J = 7.5$, 2H), 2.69 (t, $J = 6.0$ Hz, 2H), 2.62 (t, $J = 6.0$ Hz, 2H), 2.47 (t, $J = 7.3$ Hz, 2H), 2.03 to 1.78 (m, 20H), 1.63 to 1.49 (m, 4H), 1.06 (t, $J = 7.3$, 3H); MS (ESI, pos) m/z calcd. for $C_{55}H_{60}ClN_4O_3$ (M+): 859, detected: 859; HRMS (FAB) m/z calcd. for $C_{54}H_{58}ClN_4O_3$ (M+): 859.43, detected: 859.4354.

2.4 *Photophysical Properties*

For fluorescence spectroscopy analysis, dyes were dissolved in phosphate-buffered saline (PBS, pH 7.4) containing 5 g/dL bovine serum albumin (BSA) (BSA solution, pH 7.4) at a concentration of 1 μM. Emission spectra were measured following excitation at 823 nm. Absolute quantum yields were determined using a Fluorolog-3 spectrofluorometer equipped with an integrating sphere.

2.5 *Evaluation of $^1O_2$ Generation*

Estimation of $^1O_2$ generation by irradiation of dyes in PBS was conducted as reported previously.[9] Briefly, a mixture containing 180 μL PBS, 10 μL dye (200 μM) in dimethyl sulfoxide, and 10 μL singlet oxygen sensor green reagent (SOSGR, 200 μM) in MeOH was irradiated by an 830-nm LED lamp with a power density of 7.5 mW/cm^2. Fluorescence intensity of SOSGR at 525 nm was measured following excitation at 490 nm as a monitor of $^1O_2$ generation.

2.6 *In Vitro Measurement of Photoacoustic Signals*

In vitro PA signals from the dyes were measured as reported previously.[6,10] Briefly, the PA signal measurement system setup consisted of an 830-nm wavelength pulsed light for IC-*n*-T derivatives and IC7-1-Bu. The beams were generated by a Model Titanium Sapphire Laser system (Lotis TII, Minsk, Belarus) operating at 10 Hz with a 20-ns pulse duration. A transducer Model V303 (Panametrics-NDT, Waltham, Massachusetts; 1-MHz center frequency, 1-cm element size) and ultrasonic preamplifier Model 5682 (Olympus Corporation, Tokyo, Japan) collected the PA signal. A DPO3034 oscilloscope (Tektronix Company, Tokyo, Japan) was used as a gauge and light detection of the photodiode as a trigger. PA signals for IC-*n*-T derivatives and IC7-1-Bu (0.4 to 10 μM) in BSA solution were evaluated and normalized with irradiated laser intensity.

In vitro photostability was evaluated with an Endra Life Sciences Nexus 128 instrument. Dyes were dissolved in BSA solution to give a concentration of 10 μM for the analysis. Scans consisted of 60 angles with 25 pulses/angle and were performed 10 times without any intervals. The excitation wavelength was 830 nm, which was based on the absorption peak of IC-*n*-T derivatives and IC7-1-Bu. Pulse laser intensity, pulse width, and pulse frequency were 9 to 11 mJ, 7 ns, and 20 Hz, respectively. PA images were constructed as a volumetric rendering using OsiriX software. The reconstructed data were analyzed using AMIDE and normalized with respect to irradiated laser intensity. The normalized intensity (%) was calculated as a percentage of photoacoustic intensity obtained for first time measurements.

The ratio of intact to degraded IC-5-T and IC7-1-Bu after photoirradiation was investigated with RP-HPLC. IC-5-T and IC7-1-Bu were dissolved in PBS to give a concentration of 10 μM for the analysis and irradiated by an 830-nm LED lamp with a power density of 7.5 mW/cm^2. After photoirradiation, the samples were analyzed by RP-HPLC on a Cosmosil 5C_{18} column. The mobile phase of RP-HPLC was the same as described for the general synthesis procedure for compounds **9a** to **9c**.

2.7 *Cell Culture*

The human cervix adenocarcinoma cell line HeLa was obtained from American Type Culture Collection and was authenticated with the Promega PowerPlex® 16 STR system in October 2012. HeLa cells were maintained in DMEM supplemented with 10% heat-inactivated FBS, 1% penicillin and streptomycin in a humidified atmosphere containing 5% CO_2 at 37°C.

2.8 *Protein-Binding Assay*

Estimation of the dye binding site on albumin was conducted as reported previously.[5,11] Briefly, warfarin was used as a competitive inhibitor of albumin binding site I. The inhibitor (0 and 3.8 mM) was incubated for 30 min at room temperature in BSA solution. Immediately after the addition of the dyes (1 μM final concentration), the fluorescence intensity was measured following excitation at 823 nm and emission from 840 to 900 nm. The normalized intensity (%) was calculated as a percentage of fluorescence intensity obtained from samples that were not treated with inhibitor.

Binding affinities of dyes to albumin were measured as reported previously.[12] Briefly, dyes (0 to 4 μM final concentration) were incubated with BSA (4 μM) for 30 min to equilibrate. The binding affinities (K_b) of cyanine dyes to albumin can be determined using the Hill equation expressed by Eq (1) for a static quenching interaction.

$$\log[(F_0 - F)/F] = \log K_b + n \log[\text{dye}], \quad (1)$$

where n is the number of binding sites and F_0 and F are the fluorescence intensities of albumin tryptophans with or without dyes, respectively.

2.9 *In Vivo Imaging Study*

Animal experiments were conducted in accordance with institutional guidelines and approved by the Kyoto University Animal Care Committee. Female nude mice (BALB/c *nu/nu* 4-weeks old), supplied by Japan SLC, Inc., were maintained under a 12 h light/12 h dark cycle and given free access to food (D10001) and water. HeLa cells (2×10^6 cells in 100 μL of PBS) were subcutaneously inoculated into the right hind legs of mice and imaging studies were performed 14 days after transplantation.

For *in vivo* optical imaging studies performed 24 and 48 h after intravenous administration of the IC-5-T derivative (10 nmol, 100 μL), tumor-bearing mice were anesthetized with 2.5% isoflurane gas in oxygen flow (1.5 L/min) and imaged with a Clairvivo® OPT apparatus (Shimadzu Co.) with a 785-nm single laser. The power density was 1 mW/cm^2 for excitation[13] and the band-path filter for emission was 845/55 nm. Clairvivo® OPT measurement and display software version 2.6.0.1. (Shimadzu Co.) were used for imaging analysis.

In vivo PAI was performed with an Endra Life Sciences Nexus 128 instrument. A scan consisted of 120 angles with 50 pulses/angle. The excitation wavelength was 830 nm, which was based on the absorption peak of IC-*n*-T derivatives. Pulse laser intensity, pulse width, and pulse frequency were 9 to 11 mJ, 7 ns, and 20 Hz, respectively. IC-*n*-T derivatives (2.5 μmol/kg) were injected into tumor-bearing mice ($n = 3$) via the tail vein and PA images acquired 24 and 48 h after injection following administration of 2.5% isoflurane for anesthesia. PA images were constructed as a volumetric rendering using OsiriX software. PA signal intensity was calculated from the values of volumetric rendering points and normalized with respect to irradiated laser intensity. A region of interest-based analysis was performed using AMIDE.

2.10 *Statistical Analysis*

Data are expressed as means ± standard deviation. Data were analyzed with one-way factorial analysis of variance (ANOVA) followed by the Tukey test, and values with $p < 0.05$ were considered significant.

3 Results

3.1 *Synthesis of IC-n-T Derivatives*

IC-*n*-T derivatives were synthesized from cyclohexanone and 1, 1, 2-trimethyl-1H-benz[*e*]indole following a similar synthetic protocol for IC7-1-Bu, as shown in Fig. 1. Overall yields ranged from 0.1% to 0.2%.

3.2 *Photophysical Properties of IC-n-T Derivatives*

The photophysical properties of the three IC-*n*-T derivatives in BSA solution are summarized in Table 1. Each derivative showed an absorption maximum at 830 nm and an emission wavelength around 840 nm in BSA solution, which were both similar to IC7-1-Bu.

The extinction coefficients of the IC-*n*-T derivatives were around 2.0×10^5 M^{-1} cm^{-1}, and the fluorescence quantum yields around 0.05 were also similar to IC7-1-Bu. These results indicate that IC-*n*-T derivatives could be useful PAI probes since the nonradiative deactivation fraction of the absorbed light energy is available for PA signal generation.

Table 1 Photophysical properties of IC-*n*-T derivatives and IC7-1-Bu in bovine serum albumin solution.

	λ_{abs}[a] (nm)	λ_{em}[b] (nm)	Φ[c]	ε[d] (M^{-1}cm^{-1})
IC-2-T	830	845	0.04	1.8×10^5
IC-4-T	830	845	0.04	2.3×10^5
IC-5-T	830	843	0.05	2.1×10^5
IC7-1-Bu	830	843	0.06	2.4×10^5

[a]Maximum absorption wavelength.
[b]Maximum emission wavelength.
[c]Fluorescence quantum yield.
[d]Extinction coefficient.

3.3 *Evaluation of $^1O_2$ Generation Following Photoirradiation of IC-n-T Derivatives and IC7-1-Bu*

$^1O_2$ generation by photoirradiation of IC-*n*-T derivatives and IC7-1-Bu was evaluated using SOSGR, a fluorescence indicator, which reacts with $^1O_2$ selectively, resulting in an increase in 525-nm emission.[14] Figure 2 shows a significant decrease in SOSGR fluorescence intensities in solutions containing IC-*n*-T derivatives relative to the IC7-1-Bu solution. These results indicate that IC-*n*-T derivatives decreased $^1O_2$ generation by photoirradiation compared to IC7-1-Bu.

3.4 *In Vitro PA Properties of IC-n-T Derivatives and IC7-1-Bu*

We then measured the PA signal of IC-*n*-T derivatives *in vitro* to compare them with those of IC7-1-Bu. Figure 3(a) illustrates the correlation of PA signals with the dye concentration in the cuvettes. All three IC-*n*-T derivatives in BSA solution showed PA signals that were comparable to that of IC7-1-Bu.

The PA signals of the IC-*n*-T derivatives and IC7-1-Bu were measured 10 times to obtain sequential PA signal profiles, as shown in Fig. 3(b). IC-*n*-T derivatives showed smaller decreases in PA signals compared to IC7-1-Bu.

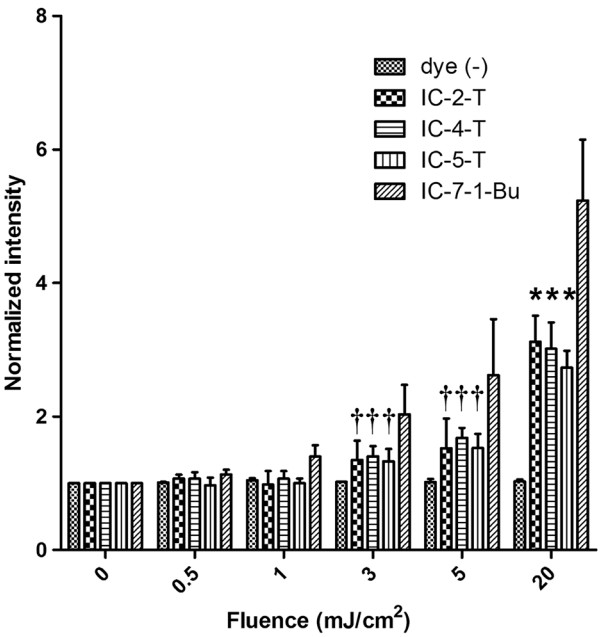

Fig. 2 Evaluation of $^1O_2$ generation by photoirradiation of IC-*n*-T derivatives and IC7-1-Bu. Normalized intensities plotted against the fluence. Comparisons were performed with one-way analysis of variance (ANOVA) followed by the Tukey test (*$P < 0.05$ versus IC7-1-Bu and dye (–), †$P < 0.05$ versus IC7-1-Bu). Data are means ± standard deviation (SD) of three independent experiments.

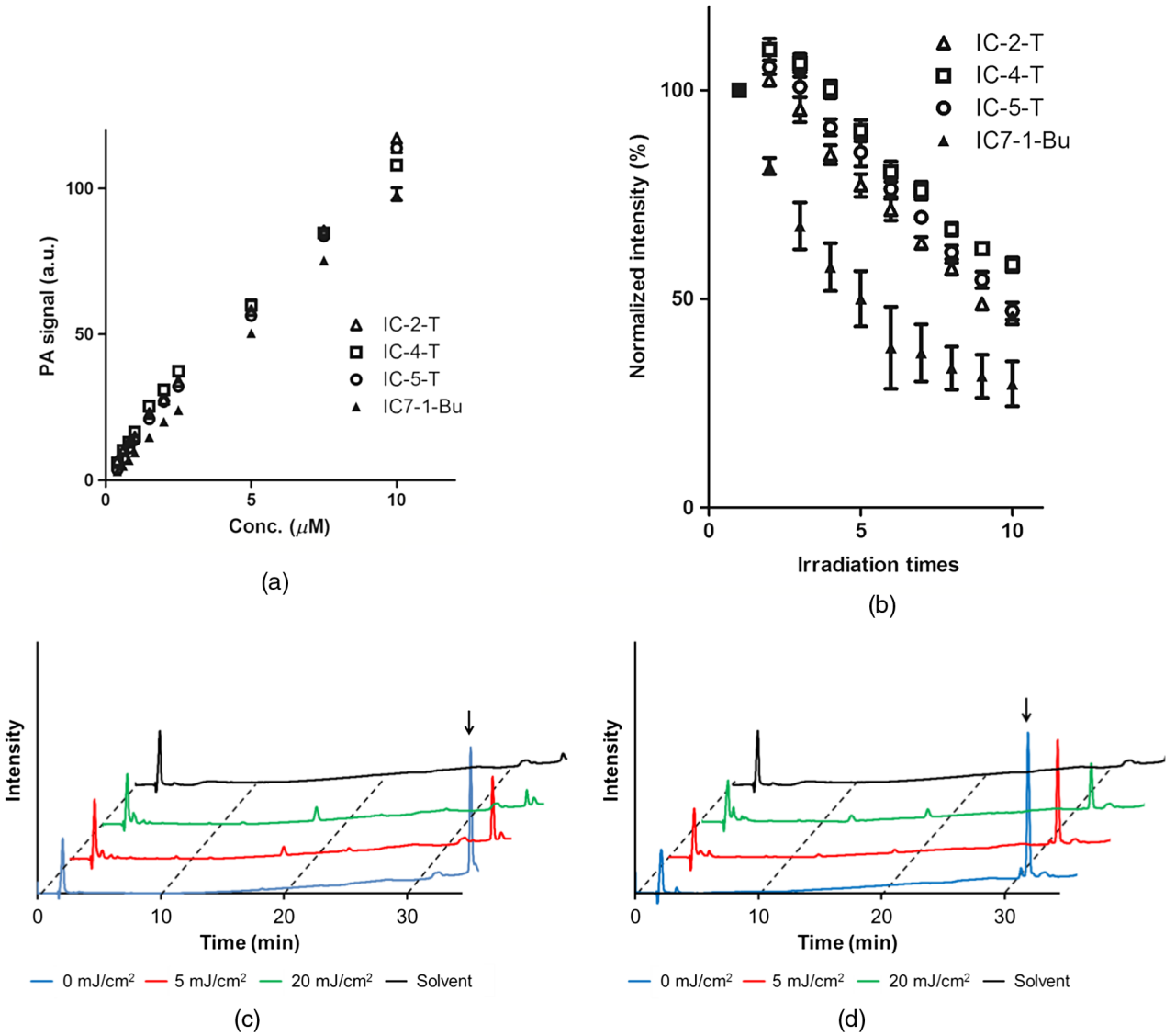

Fig. 3 *In vitro* photoacoustic (PA) properties of IC-*n*-T derivatives and IC7-1-Bu. (a) Single-time measurement of IC-*n*-T derivatives and IC7-1-Bu PA signals. PA signals were plotted against the concentrations of IC-*n*-T derivatives and IC7-1-Bu. (b) Multiple time measurement of IC-*n*-T derivatives and IC7-1-Bu PA signals. PA signals were plotted against irradiation times. Data are means ± SD of three independent experiments. (c) RP-HPLC analysis of photoirradiation of IC7-1-Bu. Arrow indicates intact IC7-1-Bu. (d) RP-HPLC analysis of photoirradiated IC-5-T. Arrows indicate intact IC-5-T.

The RP-HPLC analysis of photoirradiated IC7-1-Bu and IC-5-T is shown in Figs. 3(c) and 3(d), respectively. While $38 \pm 2\%$ of IC-5-T was intact after 20 mJ/cm^2 photoirradiation, only $10 \pm 4\%$ of intact IC7-1-Bu remained.

3.5 *Protein-Binding Assay*

The albumin-binding affinities of the dyes were measured to estimate if IC-*n*-T derivatives could be delivered to tumor sites *in vivo* using serum albumin as a drug delivery carrier as was done for an earlier study using IC7-1-Bu.[5] IC-*n*-T derivatives also bound to albumin at the warfarin binding site (Fig. 4) with IC-5-T having moderate albumin binding. Meanwhile, the other IC-*n*-T derivatives had lower albumin binding affinities relative to IC7-1-Bu (Table 2).

3.6 *In Vivo Imaging Study*

Fluorescence images of tumor-bearing mice after administration of IC-*n*-T derivatives and IC7-1-Bu clearly depicted tumors (Fig. 5). After administration, IC-5-T showed higher fluorescence intensity in the tumor region than IC-2-T and IC-4-T. The percentage of IC-*n*-T derivative fluorescence intensity that remained in the tumor region 2 days after intravenous administration was comparable to that of IC7-1-Bu (0.84 ± 0.05, 0.86 ± 0.03, 1.00 ± 0.03, and 1.04 ± 0.02 for IC-2-T, IC-4-T, IC-5-T, and IC7-1-Bu, respectively).

In vivo PAI of tumor-bearing mice after administration of IC-5-T and IC7-1-Bu also clearly depicted tumors. The percentage of the PA signal at the tumor region 2 days relative to 1 day after intravenous administration was 89% for IC-5-T and 61% for IC7-1-Bu (Fig. 6).

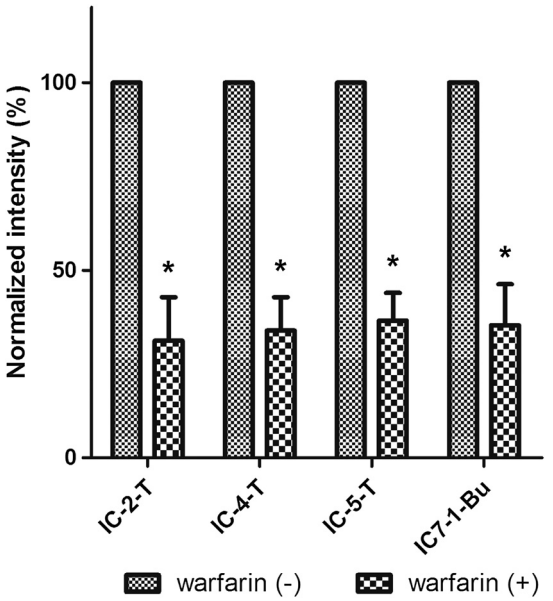

Fig. 4 Estimation of IC-*n*-T derivative protein binding. Data are means ± SD of three independent experiments. Comparisons were performed with one-way ANOVA followed by a Tukey test (*$P < 0.01$).

Table 2 Albumin-binding affinities of IC-*n*-T derivatives.

	IC-2-T	IC-4-T	IC-5-T	IC7-1-Bu
K_b ($\times 10^5$)	7.9	10	13	25

4 Discussion

In this study, we designed and synthesized IC-*n*-T derivatives to improve the photostability of IC7-1-Bu for use in *in vivo* sequential tumor imaging with PAI. An *in vitro* analysis indicated the potential of IC-*n*-T derivatives for further animal experiments because they showed improved photostabilities that were likely due to a significant decrease in $^1O_2$ levels generated by laser irradiation. Furthermore, the derivatives retained PA capacities that were comparable to IC7-1-Bu and a maximum absorbance wavelength in the NIR. In *in vivo* PAI studies, IC-5-T also clearly depicted tumors 1 and 2 days after intravenous injection, which indicates the successful improvement in photostability *in vivo*. Together, these results suggest that IC-5-T is a promising probe for *in vivo* sequential cancer imaging with PAI.

PAI has shown great promise for the early detection of cancer due to its ability to provide functional and molecular information with high resolution at clinically relevant depths, although exogenous contrast agents for *in vivo* PAI are required to increase imaging contrast and depth.[3,4] Considering the *in vivo* PAI of tumors, molecular probes should have the following characteristics: (1) photon absorption at a wavelength of 700 to 900 nm (NIR region) for high tissue permeability; (2) efficient PA signal generation; (3) high levels of probe accumulation in tumor tissues that compensate for the relatively low intrinsic sensitivity of PAI relative to optical imaging;[2,15] and (4) photostability following exposure to the high-energy laser pulses delivered during PAI.[4] In fact, our previous report showed

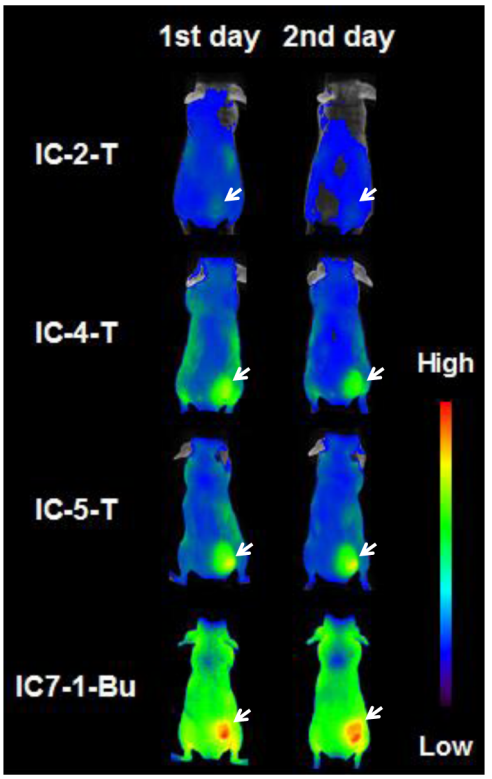

Fig. 5 *In vivo* optical imaging of IC-*n*-T derivatives and IC7-1-Bu using HeLa cell xenograft mice. Fluorescence images of HeLa cell xenograft mice 1 and 2 days after intravenous dye administration. Arrows indicate the tumor.

that IC7-1-Bu has met requirements (1), (2) and (3), and has clearly depicted tumors in *in vivo* PAI experiments with single laser irradiation.[6] In addition, the improved photostability of IC7-1-Bu should promote the usefulness of IC7-1-Bu for wider applications such as *in vivo* follow-up experiments using an identical animal to evaluate the efficacy of treatment drugs or operations by *in vivo* sequential PAI.

We selected the TSQ moiety for introduction into the IC7-1-Bu structure to improve photostability because this group should quench dye degeneration induced by the $^1O_2$ generated from energy transfer reactions between ground state triplet oxygen and triplet state dyes.[7] Indeed, the photostability of fluorescent

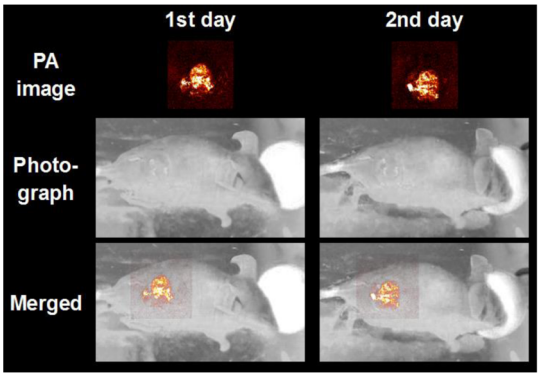

Fig. 6 *In vivo* PAI of IC-5-T using HeLa cell xenograft mice. Photoacoustic images of HeLa cell xenograft mice 1 and 2 days after intravenous administration of IC-5-T.

compounds was reportedly improved in buffer solutions containing antioxidants and TSQ at micro- to millimolar concentrations,[16,17] and the direct introduction of a moiety that functions as a photostabilizer into the fluorescent dye structure could further improve the photostability.[8] Among several TSQs that have been described, we adopted 4-nitrobenzyl alcohol derivatives because they do not require linkers for conjugation and have a small molecular size such that the TSQ should have minimal effects on important characteristics of the mother compound. Considering the site of TSQ moiety conjugation to IC7-1-Bu, a chloro group at the fluorophore center could be a candidate for the substitution, but this group can cause a large spectral shift in absorbance.[18,19] Our preliminary experiments also suggested that a compound substituted at the center of the fluorophore can change the optical properties dramatically. On the other hand, cyanine dye side chains are independent from the fluorophore and do not affect their optical properties.[5,20] Hence, we decided to introduce the 4-nitrobenzyl alcohol structure onto one of the IC7-1-Bu side chains. The results show that this drug design strategy functions well in terms of having a high capacity to quench $^1O_2$ generation and negligible effects on optical properties.

Albumin has been recognized as a useful drug delivery carrier to effectively deliver therapeutic and diagnostic agents to tumor tissues via the enhanced permeability and retention effect.[21,22] As we previously reported, after intravenous administration, IC7-1-Bu effectively accumulated in tumor tissues when serum albumin was used as a drug delivery carrier.[5] That study also showed that the side chain lengths of symmetrical cyanine dyes alter the binding affinity of the dyes to albumin and in turn the tumor targeting activity in animals. A preliminary computer simulation of IC7-1-Bu and albumin binding using the molecular modeling software MOE version 2010.10 also implied that the modification of a single alkyl chain of IC7-1-Bu would not significantly affect the albumin binding of this probe. On this basis, the length of asymmetrical cyanine side chains is important, thus we designed a series of IC-*n*-T derivatives with a butyl chain on one side and an alkyl chain with several different lengths ranging from two (IC-2-T) to five carbons (IC-5-T) on another side with the expectation that probe biodistributions would be altered in a similar fashion to that seen in our previous study.[23] While the asymmetric cyanine dye IC-*n*-T derivatives showed slightly lower albumin affinities than IC7-1-Bu, IC-5-T showed moderate fluorescence accumulation in tumors. This implies the contribution of serum albumin as a drug delivery carrier for IC-*n*-T derivatives like IC7-1-Bu, and contrary to our expectation, steric interference by the introduced moiety may have affected the albumin binding of IC-*n*-T derivatives. Since IC-5-T showed the highest albumin affinity among the IC-*n*-T derivatives, linker chains with more than five carbons may be useful to evaluate this finding. Nevertheless, it should be stressed that IC-5-T retained tumor targeting capacity at levels that were sufficient to advance *in vivo* PAI experiments.

In surgical treatment of tumors, incomplete resection often causes tumor recurrence and reduction of survival rates, thus a real-time imaging method that helps the surgeon to define microcancer locations is urgently needed to treat cancer in its earliest stages. While *in vivo* fluorescence imaging can be used for this purpose,[24,25] *in vivo* PAI has a great advantage in terms of tissue permeability and can be used to create tomographic images that are highly quantitative. These qualities suggest that PAI-based image-guided surgery (PAI-IGS)[26] may have high potential as an effective tool in early cancer diagnosis and treatment. Since IGS naturally requires sequential imaging of tumor sites of interest during the operation, PAI probes for IGS should be photostable in the face of sequential laser irradiations. In this context, the IC-5-T probe developed in this study showed reliable stability at up to $20 mJ/cm^2$ of laser irradiation, which is recognized as the maximal limit for irradiation of human skin without any harmful effects.[27] Thus, IC-5-T could be a lead compound for PAI-IGS applications.

An ideal PAI probe should be highly stable against sequential high-energy laser irradiation.[4,28] While IC-5-T showed high photostability in addition to unique characteristics as a tumor imaging probe with a low molecular weight, further improvement in IC-5-T photostability would be required to obtain quantitative and accurate tomographic images of tumor. Since nitrobenzyl groups can be degraded enzymatically,[29] the introduction of other TSQ moieties to IC7-1-Bu may be effective to develop other photostabilized dyes. In addition, cyanine dyes can reductively react with nucleophilic reagents such as primary amine and thiol compounds, which may alter their chemical forms and optical properties.[7] Indeed, cyanine dyes were reported to react with endogenously produced biomolecules, such as hydrogen sulfide and histamine, leading to altered absorption spectra.[18,19] Therefore, probe derivatization approaches, such as polyfluorination, could decrease the oxidation potential to prevent such reduction reactions and may improve cyanine dye photostability.[30] However, since further derivatization might reduce the probe's albumin binding affinity and tumor targeting ability, precise drug design that simultaneously maintains high photostability and tumor targeting capacity is required to develop ideal PAI probes.

In conclusion, we developed a novel TSQ-conjugated asymmetric cyanine dye, IC-5-T, which shows improved photostability for use in *in vivo* sequential PAI of tumors. IC-5-T demonstrated adequate PA signal generation, improved photostability through reduced $^1O_2$ generation, high tumor accumulation, and a maximum absorption peak in the NIR. These qualities suggest that IC-5-T has potential applications as an *in vivo* PAI probe for tumor imaging.

Acknowledgments

This work was supported in part by a Grant-in-Aid for Scientific Research (23113509) from the Japan Society for the Promotion of Science, and by the New Energy and Industrial Technology Development Organization (NEDO), Japan. This work was also supported in part by the Innovative Techno-Hub for Integrated Medical Bio-imaging Project of the Special Coordination Funds for Promoting Science and Technology, from the Ministry of Education, Culture, Sports, Science and Technology (MEXT), Japan. Some experiments were performed at the Kyoto University Radioisotope Research Center and Kyoto Pharmaceutical University.

References

1. L. A. Torre et al., "Global cancer statistics, 2012," *CA Cancer J. Clin.* **65**, 87–108 (2015).
2. V. Ntziachristos, "Going deeper than microscopy: the optical imaging frontier in biology," *Nat. Methods* **7**(8), 603–614 (2010).
3. L. V. Wang and S. Hu, "Photoacoustic tomography: in vivo imaging from organelles to organs," *Science* **335**(6075), 1458–1462 (2012).

4. G. P. Luke, D. Yeager, and S. Y. Emelianov, "Biomedical applications of photoacoustic imaging with exogenous contrast agents," *Ann. Biomed. Eng.* **40**(2), 422–437 (2012).
5. S. Onoe et al., "Investigation of cyanine dyes for in vivo optical imaging of altered mitochondrial membrane potential in tumors," *Cancer Med.* **3**(4), 775–786 (2014).
6. T. Temma et al., "Preclinical evaluation of a novel cyanine dye for tumor imaging with in vivo photoacoustic imaging," *J. Biomed. Opt.* **19**(9), 090501 (2014).
7. E. M. Stennett, M. A. Ciuba, and M. Levitus, "Photophysical processes in single molecule organic fluorescent probes," *Chem. Soc. Rev.* **43**(4), 1057–1075 (2014).
8. R. B. Altman et al., "Cyanine fluorophore derivatives with enhanced photostability," *Nat. Methods* **9**(1), 68–71 (2012).
9. H. Lin et al., "Feasibility study on quantitative measurements of singlet oxygen generation using singlet oxygen sensor green," *J. Fluoresc.* **23**(1), 41–47 (2013).
10. K. Kanazaki et al., "Development of human serum albumin conjugated with near-infrared dye for photoacoustic tumor imaging," *J. Biomed. Opt.* **19**(9), 096002 (2014).
11. M. Poor et al., "Fluorescence spectroscopic investigation of competitive interactions between ochratoxin A and 13 drug molecules for binding to human serum albumin," *Luminescence* **28**(5), 726–733 (2013).
12. M. Y. Berezin et al., "Rational approach to select small peptide molecular probes labeled with fluorescent cyanine dyes for in vivo optical imaging," *Biochemistry* **50**(13), 2691–2700 (2011).
13. T. Funayama et al., "Intraoperative near-infrared fluorescence imaging with novel indocyanine green-loaded nanocarrier for spinal metastasis: a preliminary animal study," *Open Biomed. Eng. J.* **6**, 80–84 (2012).
14. T. Kiesslich et al., "A comprehensive tutorial on in vitro characterization of new photosensitizers for photodynamic antitumor therapy and photodynamic inactivation of microorganisms," *BioMed Res. Int.* **2013**, 840417 (2013).
15. B. Wang et al., "Photoacoustic tomography and fluorescence molecular tomography: a comparative study based on indocyanine green," *Med. Phys.* **39**(5), 2512–2517 (2012).
16. C. E. Aitken, R. A. Marshall, and J. D. Puglisi, "An oxygen scavenging system for improvement of dye stability in single-molecule fluorescence experiments," *Biophys. J.* **94**(5), 1826–1835 (2008).
17. R. Dave et al., "Mitigating unwanted photophysical processes for improved single-molecule fluorescence imaging," *Biophys. J.* **96**(6), 2371–2381 (2009).
18. X. Wu et al., "A near-infrared fluorescence dye for sensitive detection of hydrogen sulfide in serum," *Bioorg. Med. Chem. Lett.* **24**(1), 314–316 (2014).
19. H. H. Gorris et al., "Long-wavelength absorbing and fluorescent chameleon labels for proteins, peptides, and amines," *Bioconjug. Chem.* **22**(7), 1433–1437 (2011).
20. G. Beckford et al., "The solvatochromic effects of side chain substitution on the binding interaction of novel tricarbocyanine dyes with human serum albumin," *Talanta* **92**, 45–52 (2012).
21. F. Kratz and B. Elsadek, "Clinical impact of serum proteins on drug delivery," *J. Control. Release* **161**(2), 429–445 (2012).
22. B. Elsadek and F. Kratz, "Impact of albumin on drug delivery–new applications on the horizon," *J. Control. Release* **157**(1), 4–28 (2012).
23. Y. Shimizu et al., "Development of novel nanocarrier-based near-infrared optical probes for in vivo tumor imaging," *J. Fluoresc.* **22**(2), 719–727 (2012).
24. K. Polom et al., "Current trends and emerging future of indocyanine green usage in surgery and oncology: a literature review," *Cancer* **117**(21), 4812–4822 (2011).
25. J. Yokoyama et al., "A feasibility study of NIR fluorescent image-guided surgery in head and neck cancer based on the assessment of optimum surgical time as revealed through dynamic imaging," *OncoTargets Ther.* **6**, 325–330 (2013).
26. L. Xi et al., "Photoacoustic and fluorescence image-guided surgery using a multifunctional targeted nanoprobe," *Ann. Surg. Oncol.* **21**(5), 1602–1609 (2014).
27. M. Mehrmohammadi et al., "Photoacoustic imaging for cancer detection and staging," *Curr. Mol. Imaging* **2**(1), 89–105 (2013).
28. S. Zackrisson, S. M. van de Ven, and S. S. Gambhir, "Light in and sound out: emerging translational strategies for photoacoustic imaging," *Cancer Res.* **74**(4), 979–1004 (2014).
29. K. Sharma, K. Sengupta, and H. Chakrapani, "Nitroreductase-activated nitric oxide (NO) prodrugs," *Bioorg. Med. Chem. Lett.* **23**(21), 5964–5967 (2013).
30. B. R. Renikuntla et al., "Improved photostability and fluorescence properties through polyfluorination of a cyanine dye," *Org. Lett.* **6**(6), 909–912 (2004).

Biographies for the authors are not available.